Three-Dimensional Interconnected Network of Gold Nanostructures for Molecular Sensing via Surface-Enhanced Raman Scattering Spectroscopy

Belda Amelia Junisu and Ya-Sen, Sun* (孫亞賢)

Department of Chemical and Materials Engineering, National Central University, Taoyuan 32001, Taiwan
yssun@cc.ncu.edu.tw

Abstract

This study demonstrate a template-assisted fabrication of three-dimensional interconnected network gold nanostructures (3D-NW AuNSs) for molecular sensing through surface-enhanced Raman scattering (SERS) spectroscopy. Porous templates (PTs) were fabricated by surface-reconstructed films of polystyrene-block-poly(2-vinylpyridine) (PS-*b*-P2VP) micelles. Through immersion in hot ethylene glycol, the PS-*b*-P2VP PTs composed of branched nanocylinders nanonetworks and interconnected porous channels, allowing subsequent adsorption of gold complex ions, nucleation of gold seeds, and eventual growth of AuNSs under the effects of added K_2CO_3 in aqueous solutions. Two reduction approaches were used: a) photoreduction through UV-light exposure at the nucleation stage, concurrently reduce gold complex ions (AuCIs), rapidly producing single-crystal-like gold seeds (AuSs) and stabilize the template nanodomains; b) chemical reduction by a weak reducing agent at the growth stage. Template assisted seeding growth synthesis allows 3D-NW AuNSs to have abundant thornlike protruding nanotips, providing huge surface area for the adsorption of Rhodamine 6G (R6G) molecules as well as generating a $>10^9$ enhancement factor in SERS and a low detection limit (5 nM) for adsorbed R6G.

Keywords : block copolymer, self-assembly, thin film, metallic gold nano-network, surface-enhanced Raman scattering

Introduction

New physical, chemical and optoelectronic properties of metallic gold nanostructures (AuNSs) give it important role in the fields of bio-sensing or molecular sensing through SERS-based analytical chemistry.[1-4] 3D metallic networks (3D-NW) with nanogaps and sharp protrusions can offer a highly local surface plasmon resonance (LSPR). BCPs have been widely used as supporting materials because their self-assembly can offer access to fabricating AuNSs with well-tailored morphologies and well-defined spatial order.[5,6] Despite enormous efforts in using BCP templates to fabricate 3D-NW AuNSs, synthesizing it in an effective manner remains challenging. Especially 3D-NW AuNSs, which cooperative/competitive interplays among adsorption, reduction, nucleation and growth need to be further established. This study reports a simple yet versatile BCP-templated seeding growth approach to fabricate 3D-NW AuNSs with numerous protruding nano-tips.

Experiments

3wt% solutions were prepared by dissolving $PS_{48.5k}$-*b*-$P2VP_{70k}$ powders in o-xylene. PS-*b*-P2VP micellar films were prepared on the cleaned substrates (SiO_x/Si and quartz) via spin coating from the aged solutions. The films were immersed in hot EG at 130°C for 15 min to yield network nanostructures of branched cylinders. To fabricate gold seeds (AuSs), the PTs were immersed in aqueous seed solutions that contained a mixture of 2.1 mg of $HAuCl_4.3H_2O$ and 2 mg of K_2CO_3 in 20 mL of DI water (equivalent to a 0.26 mM seed solution), and after immersion of 2h, gold complex ions (AuCIs) got adsorbed onto the templates through the electrostatic interaction of P2VP chains and precursor ions. The AuCI-adsorbed samples was imposed to UV-light irradiation in nitrogen for 6 h to produce tiny AuSs and stabilize the templates nanodomains via a cross-linking reaction. The resulting samples, denoted as AuSs@PT for brevity, were immersed in growth solutions (each of which contained a mixture of 5.5 mg of $HAuCl_4 \cdot 3H_2O$, 201.7 mg of DEA, and 6.2 mg of K_2CO_3 in 25 mL of DI water). Incubation time ranged from 1 to 5 h to grow AuNSs under stirring (300 rpm). The samples obtained after growth-solution incubation are denoted as $AuNSs^x$@PT, where superscript x represents the duration of incubation if specified. Pyrolysis at 500 °C was imposed on an $AuNSs^3$@PT sample to remove the PT, resulting in samples denoted as $AuNSs^3$.

Results

The fusion of core−shell spherical micelles during SR yields nanocylinders, some of which show undulations in shape. The PT displays a morphology of branched and interconnected nanocylinders (Figure 1a.b). The 2D GISAXS pattern (Figure 1c) shows a Debye−Scherrer ring, indicating that the PT sample has a powder-like order (the inset of Figure 1c). The 1D GISAXS profile shows broad periodic intensity oscillations. Those oscillations have a power-law intensity decay with $I \sim q_{//}^{-2.5}$ in the low-q region followed by a $q_{//}^{-1}$ dependence in intermediate $q_{//}$ region and finally a steeper intensity drop at high $q_{//}$. The power-law dependence in the low-$q_{//}$ region reflects the fractal dimension of the network while the cylinders give rise to the $q_{//}^{-1}$ dependence for the intermediate-$q_{//}$ region.[7] The simulated curve in Figure 1c shows a feature of scattering oscillations in the low-$q_{//}$ region even though its intensity decay at the high-$q_{//}$ is not obvious. The steeper intensity drop at high $q_{//}$ was not well simulated by the model, unless explained by other substructures of small size.

The nucleation of AuSs and subsequent growth of AuNSs were tailored through a template-based synthesis. A PT was soaked in the neutralized seed solution for 2h, exposed to UVIN (6h) until the full adsorption of negative AuCIs.

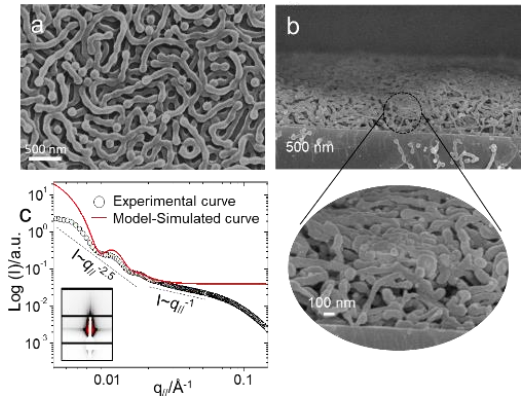

Fig. 1. Structural characterization of a PT sample obtained through SR in hot EG at 130 ºC (15 min). (a) Top-view and (b) side-view SEM images. (c) GISAXS 1D in-plane profile. The inset of Figure 1b is a zoom-in image and the inset of Figure 1c is a 2D GISAXS pattern.

The tiny AuSs with an average size of 5±2.8 nm were preferentially attached on the surface of the PT (Figure 2a). The two peaks centered at 84.1 and 87.7 eV are closer to the $4f_{7/2}$ and $4f_{5/2}$ binding energies of the bulk gold metal.[8] To grow AuNSs within a PT, AuSs@PT specimens were soaked in freshly prepared growth solutions.

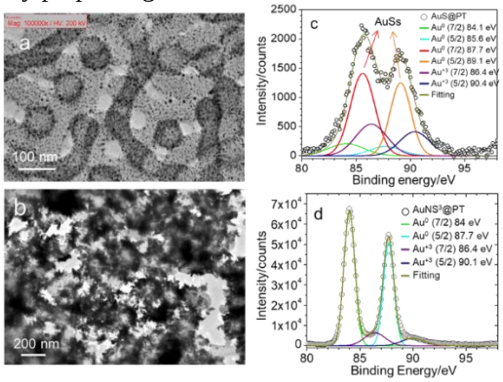

Fig. 2. (a-b) TEM images and (c-d) XPS Au_{4f} spectrum of AuSs@PT (a,c) and $AuNSs^3$@PT (b,d), respectively.

$AuNSs^3$@PT exhibits a hierarchical architecture comprises of interconnected metallic ligaments (comprised of small anisotropic nanoparticles holding together) and connective porous channels (Figure 2b). The free surface of AuNSs has abundant sharp thorn-like protrusions. Figure 2d shows a XPS spectrum together with deconvoluted curves. Two intense peaks, located at 84.0 and 87.7 eV, and weak shoulders are discernible. The peaks correspond to the $4f_{7/2}$ and $4f_{5/2}$ XPS lines of metallic gold. The shoulders at 86.4 and 90.1 eV are associated with gold oxide. Evidently, extremely minor amount of gold oxide was still present.

Discussion

The formation mechanism of AuNSs involves adsorption of ions, photoreduction of adsorbed AuCIs, nucleation of AuSs, and chemical reduction and growth of AuNSs. K_2CO_3 salts play important roles in both seed and growth solutions. They mediate the interfacial adsorption of Au ions with the P2VP chains, and control the photo-reduction of adsorbed ions, respectively. In seed solution, the $[AuCl_{4-x}(OH)_x]^-$ ions were dominant over $[AuCl_4]^-$ because of the hydrolysis of $HAuCl_4$. When a PT was soaked in neutral or acidic seed solution, incubated PT adsorbed AuCIs through electrostatic attractions. The ions were quickly reduced and nucleated to form AuSs. Soaking time in basic growth solution controls the structural evolution of AuNSs. At an initial stage of growth, discontinuous chain-like Au metallic ligaments first formed via intra-particle ripening through the photo-reduced seeds. It is likely that the intra-particle ripening of Au ligaments occurred at the expense of Cl^- (chlorine) ions in the growth solution.[11] DEA quickly interacted with $AuCl_4^-$ ions so that the hydrolysis reaction of $[AuCl_4]^-$ to $[AuCl_{4-x}(OH)_x]^-$ ions could be retarded even after K_2CO_3 addition. At the early stage, DEA mainly reduced $AuCl_4^-$ ions rather than $[AuCl_{4-x}(OH)_x]^-$ ions. As a result, intra-particle ripening driven by Cl^- ions should be dominant in crystal growth so that disconnected chain-like aggregates first formed through the photo-reduced seeds. As OH^- ions began to replace the Cl^- in the inner coordination sphere of Au^{3+} to form $[AuCl_{4-x}(OH)_x]^-$ ions, the intra-particle ripening could be suppressed because chlorine ions are expelled from the surface of AuNSs. Oppositely, at the stage of prolonged growth, the disconnected metallic ligaments started to fuse with their neighbours to form an interconnected network and thorns started to simultaneously form. The thorns formed by random attachment of small particles on the ligament surface until the porous channels are completely filled with AuNSs.

To understand the SERS performance of the obtained 3D-NW porous AuNSs, R6G was used as a molecule probe. A droplet of 10^{-5} M R6G was individually deposited on the $AuNSs^3$@PT. The Raman shifts of R6G molecules on the $AuNSs^3$@PT-covered silicon substrate are more noticeable than those on the $AuNSs^3$-covered substrate. Among the Raman shifts, the four shifts (614, 1362, 1508 and 1649 cm^{-1}) were selected for the EF calculation because of their intense intensities. The EF values are 5.8 x 10^9 (614 cm^{-1}), 5.7 x 10^9 (1362 cm^{-1}), 4.1 x 10^9 (1508 cm^{-1}) and 4.4 x 10^9 (1649 cm^{-1}) for adsorbed R6G on the $AuNSs^3$@PT. In comparison, the EFs of the four shifts excited on the $AuNSs^3$-covered substrate are relatively low, being approximately 10^8. Abundant thorns terminated on the surface of the 3D-NW AuNSs can provide surface plasmon contributions and leads to obvious Raman intensities improvement of the standard probe. The improved EFs are ascribed to increased surface area and hot-spot resonance due to the presence of protruding nano-tips.[12,13] Although the mapped 25 areas show changes in Raman intensity, it's within standard deviation < 16%. A remarkable SERS sensitivity with a very low detection limit of 5 nM for R6G molecules was attributed to the enrichment of thorns. Since the AuNSs reveal LSPR signals in the high wavelength region (500-800 nm), an excitation with laser exposure at a light wavelength in the region could amplify Raman signals through electromagnetic mechanism (EM).[3]

Acknowledgment

Financial support from the Ministry of Science and Technology (MOST 104-2221-E-008-125-MY3 and MOST 107- 2221-E-008-034-MY3) is gratefully acknowledged. We thank Dr. Yaw-Wen Yang and Dr. Chia-Hsin Wang for discussions about XPS data and for assistance in experiments at the NSRRC beamline BL24A. We thank Dr. U-Ser Jang and Dr. Chun-Jen Su for help with the GISAXS experiments at the NSRRC beamline BL23A.

References

[1] Ron, R.; Gachet, D.; Rechav, K.; Salomon, A. Direct Fabrication of 3D Metallic Networks and Their Performance. *Adv. Mater.* **2017**, *29*, 1604018.

[2] Ron, R.; Haleva, E.; Salomon, A. Nanoporous Metallic Networks: Fabrication, Optical Properties, and Applications. *Adv. Mater*. **2018**, *30*, 1706755.

[3] Tong, L.; Zhu, T; Liu, Z. Approaching the Electromagnetic Mechanism of Surface-Enhanced Raman Scattering: From Self-Assembled Arrays to Individual Gold Nanoparticles. *Chem. Soc. Rev*. **2011**, *40*, 1296-1304.

[4] Jeong, S.; Kim, M. W.; Jo, Y. R.; Kim, N. Y.; Kang, D.; Lee, S. Y.; Yim, S. Y.; Kim, B. J.; Kim, J. H. Hollow Porous Gold Nanoshells with Controlled Nanojunctions for Highly Tunable Plasmon Resonances and Intense Field Enhancements for Surface-Enhanced Raman Scattering. *ACS Appl. Mater. Interfaces* **2019**, *11*, 44458-44465.

[5] Li, C.; Jiang, B.; Chen, H.; Imura, M.; Sang, L.; Malgras, V.; Bando, Y.; Ahamad, T.; Alshehri, S. M.; Tominaka, S.; Yamauchi, Y. Superior Electrocatalytic Activity of Mesoporous Au Film Templated from Diblock Copolymer Micelles. *Nano Res.* **2016**, *9*, 1752-1762.

[6] Wang, Y.; He, C.; Xing, W.; Li, F.; Tong, L.; Chen, Z.; Liao, X.; Steinhart, M. Nanoporous Metal Membranes with Bicontinuous Morphology from Recyclable Block-Copolymer Templates. *Adv. Mater.* **2010**, *22*, 2068–2072

[7] Li, T.; Senesi, A. J.; Lee, B. Small Angle X-ray Scattering for Nanoparticle Research. *Chem. Rev.* **2016**, *116*, 11128-11180.

[8] Boyen, H. G.; Kästle, G.; Weigl, F.; Koslowski, B.; Dietrich, C.; Ziemann, P.; Spatz, J. P.; Riethmüller, S.; Hartmann, C.; Möller, M.; Schmid, G.; Garnier, M. G.; Oelhafen, P. Oxidation-Resistant Gold-55 Clusters. *Science* **2002**, *297*, 1533-1536.

[9] Jaramillo, T. F.; Baeck, S. H.; Cuenya, B. R.; McFarland, E. W. Catalytic Activity of Supported Au Nanoparticles Deposited from Block Copolymer Micelles. *J. Am. Chem. Soc.* **2003**, *125*, 7148-7149.

[10] Cuenya, B. R.; Baeck, S. H.; Cuenya, B. R.; Jaramillo, T. F.; McFarland, E. W. Size- and Support-Dependent Electronic and Catalytic Properties of Au^0/Au^{3+} Nanoparticles Synthesized from Block Copolymer Micelles. *J. Am. Chem. Soc.* **2003**, *125*. 12928-12934.

[11] Zhao, L.; Ji, X.; Sun, X.; Li, J.; Yang, W.; Peng, X. Formation and Stability of Gold Nanoflowers by the Seeding Approach: The Effect of Intraparticle Ripening. *J. Phys. Chem. C*. **2009**, *113*, 16645-16651.

[12] Zhang, L.; Lang, X.; Hirata, A.; Chen, M. Wrinkled Nanoporous Gold Films with Ultrahigh Surface-Enhanced Raman Scattering Enhancement. *ACS Nano* **2011**, *5*, 4407–4413.

[13] Wang, Y.; Becker, M.; Wang, L.; Liu, J.; Scholz, R.; Peng, J.; Gösele, U.; Christiansen, S.; Kim, D. H.; Steinhart, M. Nanostructured Gold Films for SERS by Block Copolymer-Templated Galvanic Displacement Reaction. *Nano Lett*. **2009**, *9*, 2384-2389.